# Time course study of long term biocompatibility and foreign body reaction to intraneural polyimide-based implants

Natàlia de la Oliva, Xavier Navarro, Jaume del Valle*

Institute of Neurosciences, Department of Cell Biology, Physiology and Immunology, Universitat Autònoma de Barcelona, and Centro de Investigación Biomédica en Red en Enfermedades Neurodegenerativas (CIBERNED), Bellaterra, Spain.

**Corresponding author:** Dr. Jaume del Valle, Unitat de Fisiologia Mèdica, Facultat de Medicina, Universitat Autònoma de Barcelona, E-08193 Bellaterra, Spain. E-mail: jaume.delvalle@uab.cat

**Abstract**

The foreign body reaction (FBR) is the first reaction of the nonspecific immune system against an implanted device and is characterized by the formation of a fibrotic tissue around the implant. In the case of interfaces for peripheral nerves, used to stimulate specific group of axons and to record different nerve signals, it has been shown that FBR could reduce its functionality over time due to the physical separation between nerve fibers and the interface caused by matrix deposition.

In order to understand how the FBR to intraneural interfaces evolves, polyimide non-functional devices were implanted in rat peripheral nerve. First, functional studies with electrophysiological, pain and locomotion tests demonstrate that implanted devices do not cause any alteration in nerve function. Besides, histological evaluation shows no alterations in myelinated axons or nerve architecture. Regarding the inflammatory response due to the implantation surgery, it is decreased after 2 weeks, whereas it is greater in the implanted nerves and peaks after 2 weeks. With regard to tissue deposition surrounding the implant, a tissue capsule soon appears around the devices, acquiring its maximum 2 weeks after and being remodeled subsequently. Immunohistochemical analysis reveals two different cell types implicated in the FBR in nerve: macrophages as the first cells in contact with the interface and fibroblasts that appear later on in the edge of the capsule.

## 1. Introduction

Neuroprostheses aimed to restore the loss of motor and sensory function after a limb amputation try to link the peripheral nervous system with electromechanical prostheses by means of neural electrodes. Advanced neuroprostheses rely on the capability to interface specific groups of nerve fibers within the nerve for obtaining different motor signals and for stimulating selective populations of sensory afferents. Intraneural electrodes are considered as the most adequate type, as they allow for higher selectivity of recording and stimulation, lower intensity for stimulation and increased signal-to-noise ratio of recordings compared to extraneural electrodes [(1),(2)]. Several intraneural electrodes, such as multielectrode arrays [(3)–(7)], longitudinal (LIFE) [(8),(9)] and transversal (TIME); [(10),(11)] intrafascicular electrodes have shown good performance for the bidirectional interface with the peripheral nerve. Intraneural electrodes should remain within the nerve for months or years and be able to record high quality motor nerve signals and to selectively stimulate small groups of afferent axons to evoke sensory activity for a successful performance over time Consequently, they have to show good biocompatibility and stability [(12)–(15)].

However, during chronic implantations made in human subjects, it has been observed a reduction in the functionality of electrode active sites along time [(13),(14),(16)], thus limiting the prospective use of intraneural electrodes. Such failures have been attributed to electromechanical erosion of the metal sites and fatigue of the connections, and to the biological response of the nerve tissue against the electrode implant. Regarding the latter, experimental studies have reported that the implanted electrode becomes encapsulated by host cells, creating a separation between the electrode and the nerve fibers to be interfaced [(9),(10),(17),(18)].

The foreign body reaction (FBR) is the first response of the nonspecific immune system against an implanted device. It is characterized by a primarily inflammatory phase triggered by macrophages and leukocytes, that is followed by a fibrotic phase in which fibroblasts are responsible for the formation of a fibrotic tissue around the implant [(19)]. Despite the FBR has

been widely studied and the progression of this response is well known in subcutaneous [20]–[22], peritoneal [23],[24], and even central nervous system implants [25]–[27], few studies have focused in the peripheral nervous system [28]–[30] and a detailed description of the long-term response against implanted interfaces in peripheral nerves is still needed. In order to characterize the cellular processes participating in the FBR to an intraneural electrode, which may allow to identify new targets to modulate this response and enhance the interface functionality, we have studied from 1 day to 8 months the progression of the FBR to longitudinal nerve implants made of polyimide, a material widely used in the fabrication of peripheral nerve interfaces [9],[11],[18],[31] in the rat sciatic nerve.

## 2. Material and Methods

### *2.1 Animals and surgical procedures*

Female Sprague-Dawley rats weighing 250-300g were used (n=6-8/group). All surgeries were performed under ketamine and xylacine anaesthesia (90/10 mg/kg i.p.). The sciatic nerve was surgically exposed at the midthigh and carefully freed from adherences to surrounding tissues. Passive devices of polyimide 20 mm long, 200 µm wide and 10 µm thick (Fig. 1A) were inserted longitudinally in the tibial branch of the sciatic nerve with the help of a straight needle attached to a 10-0 loop thread (STC-6, Ethicon). The thread is passed between the two arms of the device and pulls the arrow-shaped center of the electrode strip (Fig. 1B-C), as previously described for the insertion of LIFEs [9]. Longitudinal implant was chosen because of its better reproducibility in comparison with transversal implant, and to better study only the FBR inside the nerve. A group of animals underwent a sham operation with the same procedures but leaving no implant inside the nerve.

Adequate measures were taken to reduce the number of animals used and to minimize pain and animal discomfort during surgery and in the postoperative follow-up. After surgeries animals were left to recover under a warm environment and were housed at 22±2ºC under a 12:12h light cycle with food and water access ad libitum. All experimental procedures performed were approved by the Ethical Committee of the Universitat Autònoma de Barcelona in accordance with the European Communities Council Directive 2010/63/EU.

After 1, 2, 4 days and 2, 4, 8, 16 and 32 weeks post implant, animals were deeply anesthetized with an overdose of pentobarbital and perfused transcardially with 4% PFA in phosphate buffer (PB). After the perfusion, the sciatic nerve segment including the implant was collected and kept in 30% sucrose in PB for immunohistochemistry, in 70% ethanol for paraffin embedding or in 3%glutaraldehyde-3% paraformaldehyde in PB for light and electron microscopy.

*2.2 Functional evaluation*

The functional properties of the nerves that had been implanted were evaluated by means of nerve conduction, algesimetry and locomotion tests along time after the implant. Nerve conduction test was performed by stimulating the sciatic nerve proximally with single electrical pulses and recording the compound muscle action potentials (CMAPs) of the gastrocnemius medialis (GM) muscle as previously described [18]. The nociceptive threshold to mechanical stimuli was evaluated by means of an electronic Von Frey algesimeter (Bioseb, Chaville, France) following the same protocol described before [32]. Rats were placed on a wire net platform in plastic chambers, and a metal tip applied to the sole of the hindpaw until the rat withdrew the paw in response to the stimulus. The walking track test was performed to assess locomotor function after the implant. The plantar surface of the hindpaws was painted with black ink and the rat was left to walk along a corridor. The print length, the distance between the 1st and 5th toes and between the 2nd and 4th toes were measured to calculate the Sciatic Functional Index (SFI) [33].

*2.3 Morphological evaluation*

In order to evaluate the microstructure of the implanted nerves and the myelinated nerve fibers, segments fixed in 3% glutaraldhyde-3% paraformaldehyde were postfixed in 2% $OsO_4$ for 2h, dehydrated through ethanol series and embedded in epon resin. Semithin sections (0.5 μm thick) were stained with toluidine blue and examined by light microscopy. The number of myelinated fibers in the implanted tibial nerve was counted in images taken at 100x chosen by systematic random sampling of squares representing at least 30% of the nerve cross-sectional area. The cross-sectional area of the whole sciatic nerve was measured at 4x with a microscope BX51 (Olympus) and a DP73 digital camera (Olympus) and the total number of myelinated fibers estimated. The thickness of the deposited tissue around the implant was measured as the distance between each side of the device and the closest myelinated axon, using ImageJ software [34].

Transmission electron microscopy (TEM) was used to evaluate the ultrastructure of the tissue and collagen deposition around the polyimide device in transverse nerve sections. Ultrathin sections of the entire nerve were cut, mounted on formvar 200 mesh copper grids and contrasted with uranyl acetate/lead citrate. A TEM microscope (JEM 1400) was used to take pictures of the area with the implanted device, to analyse the encapsulating tissue and the surrounding nerve fibers at different time points.

*2.4 Immunohistochemistry*

Nerve segments containing the implanted polyimide device were serially cut in 15 µm thick sections in 10 slides with 12 slices each with a cryostat (Leica CM190, Leica Microsystems). Nerve sections were blocked with normal donkey serum and incubated overnight at 4ºC with primary antibodies rabbit anti-iba1 (Wako, 191947, 1:500) and mouse anti-CD-68 clone ED1 (abcam, ab31630, 1:500) for macrophages and mouse anti-CD90 clone OX-7 (BD Pharmingen, 554897, 1:150) for fibroblasts. Slides were then washed with 0.1% Tween 20 buffer solution and incubated with AlexaFluor 594 donkey anti-rabbit (Invitrogen, A21207, 1:200) and 488 donkey anti-mouse (Invitrogen, A21202, 1:200) secondary antibodies for 1 h at room temperature. Finally, sections were mounted with mowiol containing DAPI (0.1 µg/ml, Sigma).

To quantify the amount of infiltrating macrophages, images of the whole tibial nerve with iba1 or ED1 immunostaining were taken with an epifluorescence microscope BX51 (Olympus) attached to a DP73 digital camera (Olympus) and equally treated to adjust brightness and contrast. Then, the background was subtracted and a threshold of detection and binarization was applied. Iba1 or ED1 positive cells were counted in the whole area of the tibial nerve, excluding the implant device and the tissue capsule using the command "Analyze Particles" of ImageJ.

*2.5 Paraffin embedding and hematoxylin-eosin staining*

To determine the amount of foreign body giant cells (FBGCs) around the implant, nerve segments containing the implanted device were dehydrated with increasing ethanol series, followed by increasing xylene series and finally embedded in paraffin. Then, 5 µm thick serial sections were cut with a microtome (Leica RM 2255). To study FBGCs, slides were deparaffinized using two xylene rinses of 15 min each and rehydrated with decreasing ethanol series and 5 min in water. Then, slides were immersed in hematoxylin Harris solution (Fluka, Sigma) for 7 min and washed in water followed by 1% HCl in ethanol solution for 20 sec. Finally, sections were washed again with water and stained with Eosin Y (Merck Millipore) for 5 min. Sections were dehydrated with series of graded ethanol rinses and mounted with DPX (Sigma). Then, the number of FBGC was counted under the microscope in each stained section, and expressed as FBGC per mm of implant length. Moreover, pictures of every FBGC were taken and the diameter was measured with ImageJ.

*2.6 Statistical analysis*

Results are expressed as mean ± SEM. Means were compared with one or two-way ANOVA followed by Bonferroni post hoc test for differences between groups or times. To quantify the linear relationship between two variables, the Pearson's correlation coefficient and the P-value of the Fisher test were calculated. All analysis were conducted by using GraphPad Prism software. Statistical significance was considered when $p < 0.05$.

## 3. Results

### *3.1 Longitudinal neural implants do not cause damage in the implanted nerves*

Functional studies performed along time (from week 1 up to month 8) postimplant did not show any changes in nerve conduction, pain thresholds or locomotion (Supplementary Fig. 1). Histological evaluation of polyimide implanted nerves revealed that all the implanted devices were placed within the tibial nerve (Fig. 2A). Light microscopy observations showed a normal fascicular architecture and axonal morphology of both implanted and sham nerves, similar to intact sciatic nerves (Fig. 2A-B) and the number of myelinated fibres showed no differences between groups (Fig. 2C). Moreover, no signs of axonal degeneration or demyelination due to the surgery or the implanted device within the nerve were found, indicating that the implant model used was useful to assess the FBR to the polyimide device, without confounding factors that might be due to tissue damage.

### *3.2 Nerve response and tissue capsule formation*

The tissue capsule formed around the implant was evaluated under light microscopy. Whereas in the sham nerves there was no evidence of wound or tissue aggregation at any time point (Fig. 3B), the surrounding of the implant was rapidly modified in the device implanted nerves (Fig. 3A). Quantification of tissue deposition thickness around the implant exhibited a gradual increase from 2 days to 2 weeks post-implant when it reached its maximum, and a slight decrease and compaction thereafter (Fig. 3C).

Detailed analysis of the encapsulating tissue under light and transmission electron microscopy showed several changes in the surroundings of the device. Thus, at day one only some erythrocytes could be seen near the implant and axons were still in close contact with the polyimide. After 4 days, some amoeboid cells had already arrived to the polyimide device vicinity (Fig. 4A) and started to be organized creating a small gap between the implant and the axons. After 2 and 4 weeks post implant, the capsule that separated the axons and the

polyimide implant appeared as a more compacted tissue containing mainly amoeboid-shaped cells and the characteristic collagen deposition of the endoneurium can no further be distinguished in the surroundings of the implant (Fig. 4B&D). At 8 weeks, two zones could be differentiated in the encapsulating tissue, with an inner area stocked with amoeboid cells as in the previous time points and an outer region composed of layers of parallel spindle-shaped cells (Fig. 4C&E). While this disposition was very similar after 16 weeks, the presence of amoeboid cells seemed to slightly decline, but it was at 32 weeks post implant that only spindle-shape cells were seen in the capsule (Fig. 4F) with no presence of amoeboid cells. Moreover, these changes in the cellular type from 8 to 32 weeks also correlated with a further organization of the extracellular matrix of the capsule, with an increasing deposition and gradual organization of new collagen fibers that progressively invaded the area former occupied by spindle-shaped and amoeboid cells (Fig. 4D-F and insets).

*3.3 Cellular characterization of the FBR*

To evaluate the inflammatory response due to the surgery or the implant, we assessed the presence of Iba1 labeled macrophages in the whole tibial nerve. Whereas in intact nerves a few macrophages were seen, the number of Iba1 positive macrophages started to increase within the implanted nerves one day after surgery both in polyimide device and in sham groups (Fig. 5A-B). The inflammatory response caused solely by the surgery, evaluated in sham rats, peaked at 4 days and decreased noticeably at 2 and 4 weeks, reaching similar values than intact animals from week 8 onwards (Fig. 5C). In contrast, the inflammatory reaction due to the implanted device peaked at 2 weeks and took more time to resolve, with a slight decrease at 4 weeks that persisted 8 weeks after the implant. Finally, at week 16 and 32, the number of macrophages showed a further decrease but with still significantly more $Iba1^{+}$ cells than sham and intact animals (Fig. 5C). Moreover, to characterize these infiltrating macrophages, the amount of macrophages that presented positivity for the CD-68 ED1 antigen (Supplementary Fig. 2A) was quantified. As expected, all the CD-68 positive cells

were also stained with the Iba1 antibody, while several Iba1$^+$ macrophages did not express the ED1 antigen, showing a similar pattern of evolution than Iba1 labeling (Supplementary Fig. 2B) with a peak at 2 weeks after the implantation and a gradual decline up to 8 months. Hence, the amount of CD-68$^+$ and Iba1$^+$ cells followed a direct relationship (supplementary Fig. 2C) with a slope statistically significant different from zero (F-test).

To further investigate how the tissue capsule is formed around the implant, we focused on the two main cell populations involved in the FBR process: macrophages and fibroblasts [35]. In the host response in the implanted peripheral nerves, macrophages were the first cells to arrive (Fig. 6A) and rapidly surround the device from day 2-4 up to 4 weeks after implant (Fig. 6B-E). Indeed, after 2 and 4 weeks, the capsule around the device was mainly formed by compacted macrophagic cells expressing Iba1 in close contact with the device, in a similar disposition of the round-shape cells observed by TEM in figure 4. By week 8, some CD90+ fibroblasts started to appear in the edge of the capsule, between the inner macrophage layer and the surrounding nerve fibres (Fig. 6F), confirming the observations of light and electron microscopy. After 16 weeks, although the number of cells in the capsule decreased, Iba1 positive macrophages were still in contact with the device and CD90 positive fibroblasts were in the outer layer of the capsule, in contact with nerve fibres (Fig. 6G). After 32 weeks of implant, most cells in the capsule were CD90 positive fibroblasts within a well-organized extracellular matrix (Fig 6H).

Finally, the amount of FBGC was also measured as another hallmark of FBR. These cells resulting from macrophage fusion appeared soon after the polyimide device implantation and its number increased over time (Fig. 7A-B). The FBGC seen in this model had many nuclei mainly in the cellular periphery [36], as expected with the presence of foreign bodies. By week 2 these cells were easily recognizable around the implant, becoming stabilized in number and size (Fig. 7B-C) up to 8 weeks. From week 16 onwards, the amount of these cells started to decline concomitantly with the emergence of fibroblasts and the decline of macrophages both in the nerve and the capsule.

## 4. Discussion

After the implant of any biomaterial in the body, early and chronic cellular and tissue responses occur [19],[37]. These events include an inflammatory response, foreign body reaction, and fibrous encapsulation of the implanted devices [38],[39]. The peripheral nervous system is not an exception [9] and it is a serious problem when the active sites of implanted intraneural interfaces have to be in intimate contact with nerve fibers to have a proper functionality. Although many studies have reported good results regarding stimulation and recording of nerve signals in short-term studies, a progressive loss of function of intraneural electrodes that reduce the useful life of the interface has been usually reported and attributed, at least in part, to the FBR [13],[14],[16],[29].

Some reports have characterized the FBR to intraneural implants in cats [30] or in humans [28], but these studies were conducted after implantation of rigid multielectrode Utah slanted arrays and the stiffness of these electrodes has been reported to contribute to traumatic nerve injuries produced by mechanical tension and an increased FBR [40]. However, here we describe in detail the progression of the FBR to longitudinal intraneural devices fabricated with polyimide, a flexible material that can deform in 3D and adapt with the nerve [41], widely used in the fabrication of nerve electrodes implanted in rats [18],[42],[43] and in humans[13]–[15]. Therefore, the information in this study may help to design novel strategies for modulating the FBR against electrodes placed within the peripheral nerve. Besides, although the central nervous system reacts different to neural implants due to the different populations implicated in this response [26],[44],[45], the information provided here could also be used to understand and treat similar reactions in the CNS.

Unlike other fibrotic responses in pathological conditions where scar tissue impairs proper function of the organ [46],[47], our results showed that the new tissue formation in the peripheral nerve does not have a negative impact on its function after careful implantation, as previously reported when implanting longitudinal (LIFE) [9] or even transversal (TIME) electrodes [10]. Electrophysiological tests of the implanted nerves did not show alterations in

the onset and the amplitude of the evoked compound action potentials along the 8 months of implantation. Besides, there were no functional alterations observed in nociceptive and in locomotion tests. These results were corroborated by histological observations of implanted and sham nerves, where the normal fascicular architecture was preserved, and no evidences of axonal damage and distal degeneration were observed at all the studied time points. This is an important point, since the longitudinal implant of the thin film polyimide device, mimicking the use of tf-LIFEs, allowed us to investigate the FBR against the device, without relevant contributions of tissue damage due to the surgical procedure or to the mechanical stress of connected wires.

In order to understand how the FBR evolves, we first studied the infiltration of macrophages in the nerve as a sign of the immune response. Whereas in the sham group the inflammatory reaction was low and took short time to resolve, in the device implanted group there were more infiltrating macrophages and the inflammation was longer in time, becoming chronic. This evolution corresponds to the FBR widely studied in other tissues, which normally has an acute inflammatory phase that becomes chronic with time [19]. Moreover, the evolution of $ED1^+$ macrophages labelling suggests that there are no changes in the responsiveness of these cells with time as they appear and disappear following the same pattern of evolution than the pan macrophage marker Iba1[48]. Hence, the linear correlation of ED1/$Iba1^+$ cells indicates that after the implantation of PI longitudinal devices, there is not a differential rate of macrophage reactivity rather than an increase and a subsequent decrease of both $Iba1^+$ and $ED1^+$ macrophages.

We also assessed the progressive formation of an encapsulating tissue around the polyimide device. One day after the implantation the body started to react against the foreign device with changes in the surrounding as seen by electron microscopy. Nevertheless, there was no real capsule until four days and the thickness peaked by 2 weeks. From week 4 to the end of the follow-up, the capsule was progressively decreasing in thickness until stabilization. This dynamic in the capsule formation is coincident in time with the infiltration of macrophages in

the nerve due to the implant described here which also peaked after 2 weeks and started to decrease thereafter [49]. It has been shown that macrophages and phagocytes are related with the nature of the material implanted and its degradation dynamics [50],[51]. Thus, biodegradable materials would stimulate a more M1 and phagocytic environment to eliminate the implant. In contrast, non-biodegradable materials would stimulate a more M2, pro-fibrotic and tissue remodeling environment, with the contribution of FBGC and matrix deposition. In fact, fused macrophages forming FBGCs were found surrounding the implanted device as early as 1 day after the implant contributing to the FBR and their size did not change substantially throughout the study. The amount of these cells increased gradually to reach a maximum at 2 weeks, similar to the maximum of $Iba1^+$ cells and capsule thickness but the number of these declined more slowly than macrophages in the nerve at 4 or 8 weeks. And it is only at 16 or 32 weeks, when macrophages have practically disappeared that the presence of these cells also decline as a hallmark of the chronic phase of the FBR [39]. However, FBGCs are found only within the tissue capsule where tissue reactivity and inflammation is higher than within the nerve endoneurium, and these cells have been linked to the tissue formation around implants [52]: Therefore, the subsequent decline of FBGC after macrophage drop could indicate an intermediate step between macrophage to fibroblast presence around the implant when the tissue capsule switches from a phagocytizing state to a barrier forming state due to the presence of a non-phagocytable foreign body. Taking our results into account, polyimide intraneural implants could be stimulating the second scenario, regarding the presence of FBGC and the early resolution of the inflammatory response in the nerve in comparison to the remodeling response. Nevertheless, a deeper analysis of the molecular environment and the degradation process of the different implanted devices would further increase the understanding of the relationship between the foreign body and the peripheral nerve.

Moreover, the changes in the cellular and the molecular characteristics of the capsule in the nerve seem to follow a similar pattern as the FBR in subcutaneous implants [38] although the

evolution may be different from what has been previously described for FBR in the nerve[42],[53]. Thus, during the acute inflammatory phase of the FBR, macrophages and other immune cells, such as mast cells and neutrophils, start to surround the foreign body and to adsorbed proteins on the device surface in a process called biofouling that will stimulate the subsequent phases [38]. The accumulation of these cells around the device would contribute to the pro-inflammatory environment which leads the subsequent chronic inflammation and tissue remodeling phase [19]. During the first weeks after the intraneural implants, there is a marked presence of round-shaped Iba1$^{+}$ macrophages surrounding the implanted device. Besides, no evidence of organized matrix or collagen production near the device can be seen under electron microscopy. Progressively over time, more macrophages surround the device and, from 8 weeks onwards, fibroblasts arise at the edge of the capsule. Later on, the occurrence of macrophages starts to decline while fibroblasts increase their presence at 16 weeks. Finally, 8 months after the implantation, macrophages almost disappear from the encapsulating tissue and fibroblasts become more numerous and form a permanent connective capsule. These changes in the cellularity of the capsule correlate with an increase in collagen production and organization of the matrix. While other studies of the FBR to intraneural microelectrodes [29],[30] have shown the presence of macrophages surrounding the device but no alterations in the axons near the electrode, here we also demonstrate the implication of fibroblasts in the formation of the capsule and how it coincides in time with the increase in organization of the new extracellular collagen matrix.

In conclusion, several efforts have been reported to improve biomaterial characteristics and to understand the underlying mechanisms of the FBR against implantable devices for other tissues than the nerve [50],[54],[55]. Our results describe how the FBR against a polyimide implant in the peripheral nerve occurs and which are the main players. The understanding of these changes will let to a better development of new strategies that would reduce the FBR against intraneural implants and thus lengthen their lifespan.

**Acknowledgements**

This research was supported by the European Union FPT-ICT project NEBIAS under contract number 611687, FEDER funds, and TERCEL (RD12/0019/0011) and CIBERNED (CB06/05/1105) funds from the Instituto de Salud Carlos III of Spain. The authors thank Monica Espejo and Jessica Jaramillo for the technical help and Servei de Microscopia (UAB) for its help with TEM images. The authors would like to express their special appreciation to Matthias Müeller and Thomas Stieglitz from IMTEK for providing the polyimide devices.

**References**


1. Yoshida K, Pellinen D, Pivin D, Rousche P, Kipke D. Development of the thin-film longitudinal intrafascicular electrode. Proc 5th Annu Conf IFESS. 2000;279.

2. Badia J, Boretius T, Andreu D, Azevedo-Coste C, Stieglitz T, Navarro X. Comparative analysis of transverse intrafascicular multichannel, longitudinal intrafascicular and multipolar cuff electrodes for the selective stimulation of nerve fascicles. J Neural Eng. 2011;8:36023.

3. Branner A, Normann RA. A multielectrode array for intrafascicular recording and stimulation in sciatic nerve of cats. Brain Res Bull. 2000;51:293–306.

4. Branner A, Stein RB, Normann RA. Selective stimulation of cat sciatic nerve using an array of varying-length microelectrodes. J Neurophysiol. 2001;85:1585–94.

5. Clark GA, Ledbetter NM, Warren DJ, Harrison RR. Recording sensory and motor information from peripheral nerves with Utah Slanted Electrode Arrays. Proc Annu Int Conf IEEE Eng Med Biol Soc EMBS. 2011;4641–4.

6. Wark HA, Sharma R, Mathews KS, Fernandez E, Yoo J, Christensen MB, Tresco P, Rieth L, Solzbacher F, Normann R a, Tathireddy P. A new high-density (25 electrodes/mm$^2$) penetrating microelectrode array for recording and stimulating sub-millimeter neuroanatomical structures. J Neural Eng. 2013;10:45003.

7. Clark GA, Wendelken S, Page DM, Davis T, Wark HAC, Normann RA, Warren DJ, Hutchinson DT. Using multiple high-count electrode arrays in human median and ulnar nerves to restore sensorimotor function after previous transradial amputation of the hand. 2014 36th Annu Int Conf IEEE Eng Med Biol Soc EMBC 2014. 2014;1977–80.

8. Malmstrom J, McNaughton T, Horch K. Recording properties and biocompatibility of chronically implanted polymer-based intrafascicular electrodes. Ann Biomed Eng. 1998;26:1055–64.

9. Lago N, Yoshida K, Koch KP, Navarro X. Assessment of biocompatibility of chronically

implanted polyimide and platinum intrafascicular electrodes. IEEE Trans Biomed Eng. 2007;54:281–90.

10. Badia J, Boretius T, Pascual-Font A, Udina E, Stieglitz T, Navarro X. Biocompatibility of chronically implanted transverse intrafascicular multichannel electrode (TIME) in the rat sciatic nerve. IEEE Trans Biomed Eng. 2011;58:2324–32.

11. Boretius T, Badia J, Pascual-Font A, Schuettler M, Navarro X, Yoshida K, Stieglitz T. A transverse intrafascicular multichannel electrode (TIME) to interface with the peripheral nerve. Biosens Bioelectron. Elsevier B.V.; 2010;26:62–9.

12. Dhillon GS, Horch KW. Direct neural sensory feedback and control of a prosthetic arm. IEEE Trans Neural Syst Rehabil Eng. 2005;13:468–72.

13. Rossini PM, Micera S, Benvenuto A, Carpaneto J, Cavallo G, Citi L, Cipriani C, Denaro L, Denaro V, Di Pino G, Ferreri F, Guglielmelli E, Hoffmann KP, Raspopovic S, Rigosa J, Rossini L, Tombini M, Dario P. Double nerve intraneural interface implant on a human amputee for robotic hand control. Clin Neurophysiol. International Federation of Clinical Neurophysiology; 2010;121:777–83.

14. Raspopovic S, Capogrosso M, Petrini FM, Bonizzato M, Rigosa J, Di Pino G, Carpaneto J, Controzzi M, Boretius T, Fernandez E, Granata G, Oddo CM, Citi L, Ciancio a. L, Cipriani C, Carrozza MC, Jensen W, Guglielmelli E, Stieglitz T, Rossini PM, Micera S. Restoring Natural Sensory Feedback in Real-Time Bidirectional Hand Prostheses. Sci Transl Med. 2014;6:222ra19-222ra19.

15. Oddo CM, Raspopovic S, Artoni F, Mazzoni A, Spigler G, Petrini F, Giambattistelli F, Vecchio F, Miraglia F, Zollo L, Di Pino G, Camboni D, Carrozza MC, Guglielmelli E, Rossini PM, Faraguna U, Micera S. Intraneural stimulation elicits discrimination of textural features by artificial fingertip in intact and amputee humans. Elife. 2016;5:1–27.

16. Warwick K, Gasson M, Hutt B, Goodhew I, Kyberd P, Abdrews B, Teddy P, Shad A.

The application of implant technology for cybernetic systems. Arch Neurol. 2003;60:1369–73.

17. Branner A, Stein RB, Fernandez E, Aoyagi Y, Normann RA. Long-Term Stimulation and Recording with a Penetrating Microelectrode Array in Cat Sciatic Nerve. IEEE Trans Biomed Eng. 2004;51:146–57.

18. Cutrone A, Del Valle J, Santos D, Badia J, Filippeschi C, Micera S, Navarro X, Bossi S. A three-dimensional self-opening intraneural peripheral interface ( SELINE ). J Neural Eng. IOP Publishing; 2015;12:0.

19. Anderson JM, Rodriguez A, Chang DT. Foreign body reaction to biomaterials. Semin Immunol. 2008.

20. Gretzer C, Emanuelsson L, Liljensten E, Thomsen P. The inflammatory cell influx and cytokines changes during transition from acute inflammation to fibrous repair around implanted materials. J Biomater Sci Polym Ed. 2006;17:669–87.

21. Fet N, Alizai PH, Fragoulis A, Wruck C, Pufe T, Tolba RH, Neumann UP, Klinge U. In vivo characterisation of the inflammatory reaction following mesh implantation in transgenic mice models. Langenbecks Arch Surg. Springer Verlag; 2014;399:579–88.

22. Kastellorizios M, Papadimitrakopoulos F, Burgess DJ. Multiple tissue response modifiers to promote angiogenesis and prevent the foreign body reaction around subcutaneous implants. J Control Release. 2015;214:103–11.

23. Robitaille R, Dusseault J, Henley N, Desbiens K, Labrecque N, Hall?? JP. Inflammatory response to peritoneal implantation of alginate-poly-L-lysine microcapsules. Biomaterials. 2005;26:4119–27.

24. Le SJ, Gongora M, Zhang B, Grimmond S, Campbell GR, Campbell JH, Rolfe BE. Gene expression profile of the fibrotic response in the peritoneal cavity. Differentiation. Elsevier; 2010;79:232–43.

25. Biran R, Martin DC, Tresco PA. Neuronal cell loss accompanies the brain tissue

response to chronically implanted silicon microelectrode arrays. Exp Neurol. 2005;195:115–26.

26. Polikov VS, Tresco PA, Reichert WM. Response of brain tissue to chronically implanted neural electrodes. J Neurosci Methods. 2005;148:1–18.

27. Yanagihara T, Goldstein NP, Svien HJ, Bahn RC. Foreign body reaction of the brain: Enzyme-histochemical study in dogs. Neurology. 1967;17:337.

28. Christensen MB, Wark HA, Hutchinson DT. A histological analysis of human median and ulnar nerves following implantation of Utah slanted electrode arrays. Biomaterials. Elsevier Ltd; 2016;77:235–42.

29. Wark HA, Mathews KS, Normann RA, Fernandez E. Behavioral and cellular consequences of high-electrode count Utah Arrays chronically implanted in rat sciatic nerve. J Neural Eng. 2014;11:46027.

30. Christensen MB, Pearce SM, Ledbetter NM, Warren DJ, Clark GA, Tresco PA. The foreign body response to the Utah Slant Electrode Array in the cat sciatic nerve. Acta Biomater. Acta Materialia Inc.; 2014;10:4650–60.

31. Rubehn B, Stieglitz T. In vitro evaluation of the long-term stability of polyimide as a material for neural implants. Biomaterials. Elsevier Ltd; 2010;31:3449–58.

32. Santos D, Wieringa P, Moroni L, Navarro X, Del Valle J. PEOT/PBT Guides Enhance Nerve Regeneration in Long Gap Defects. Adv Healthc Mater. 2017;6.

33. de Medinaceli L, Freed WJ, Wyatt RJ. An index of the functional condition of rat sciatic nerve based on measurements made from walking tracks. Exp Neurol. 1982;77:634–43.

34. Schneider C a, Rasband WS, Eliceiri KW. NIH Image to ImageJ: 25 years of image analysis. Nat Methods. Nature Publishing Group; 2012;9:671–5.

35. Anderson JM. Future challenges in the *in vitro* and *in vivo* evaluation of biomaterial

biocompatibility. Regen Biomater. 2016;rbw001.

36. McNally AK, Anderson JM. Macrophage fusion and multinucleated giant cells of inflammation. Adv Exp Med Biol. 2011;713:97–111.

37. Luttikhuizen DT, Harmsen MC, Van Luyn MJA. Cellular and molecular dynamics in the Foreign Body Reaction. Tissue Eng. 2006;10:77–96; discussion 97.

38. Ward KW. A review of the foreign-body response to subcutaneously-implanted devices: the role of macrophages and cytokines in biofouling and fibrosis. J diabetes Sci Technol. 2008;2:768–77.

39. Sheikh Z, Brooks PJ, Barzilay O, Fine N, Glogauer M. Macrophages, Foreign Body Giant Cells and Their Response to Implantable Biomaterials. Materials (Basel). 2015;8:5671–701.

40. Lacour SP, Benmerah S, Tarte E, FitzGerald J, Serra J, McMahon S, Fawcett J, Graudejus O, Yu Z, Morrison B. Flexible and stretchable micro-electrodes for in vitro and in vivo neural interfaces. Med Biol Eng Comput. 2010;48:945–54.

41. del Valle J, Navarro X. Interfaces with the peripheral nerve for the control of neuroprostheses. Int Rev Neurobiol. 2013;109:63–83.

42. Wurth S, Capogrosso M, Raspopovic S, Gandar J, Federici G, Kinany N, Cutrone A, Piersigilli A, Pavlova N, Guiet R, Taverni G, Rigosa J, Shkorbatova P, Navarro X, Barraud Q, Courtine G, Micera S. Long-term usability and bio-integration of polyimide-based intra-neural stimulating electrodes. Biomaterials. Elsevier Ltd; 2017;122:114–29.

43. Delgado-Martínez I, Righi M, Santos D, Cutrone A, Bossi S, D'Amico S, Del Valle J, Micera S, Navarro X. Fascicular nerve stimulation and recording using a novel double-aisle regenerative electrode. J Neural Eng. 2017;in press.

44. Moshayedi P, Ng G, Kwok JCF, Yeo GSH, Bryant CE, Fawcett JW, Franze K, Guck J. The relationship between glial cell mechanosensitivity and foreign body reactions in

the central nervous system. Biomaterials. Elsevier Ltd; 2014;35:3919–25.

45. Seymour JP, Kipke DR. Neural probe design for reduced tissue encapsulation in CNS. Biomaterials. 2007;28:3594–607.

46. Duffield JS. Cellular and molecular mechanisms in kidney fibrosis. J Clin Invest. 2014;124:2299–306.

47. Gross TJ, Hunninghake GW. Idiopathic pulmonary fibrosis. English J. 2001;345:517–25.

48. Ito D, Tanaka K, Suzuki S, Dembo T, Fukuuchi Y. Enhanced expression of Iba1, ionized calcium-binding adapter molecule 1, after transient focal cerebral ischemia in rat brain. Stroke. 2001;32:1208–15.

49. Williams PL, Hall SM. Chronic Wallerian degeneration--an in vivo and ultrastructural study. J Anat. Wiley-Blackwell; 1971;109:487.

50. Veiseh O, Doloff JC, Ma M, Vegas AJ, Tam HH, Bader AR, Li J, Langan E, Wyckoff J, Loo WS, Jhunjhunwala S, Chiu A, Siebert S, Tang K, Hollister-Lock J, Aresta-Dasilva S, Bochenek M, Mendoza-Elias J, Wang Y, Qi M, Lavin DM, Chen M, Dholakia N, Thakrar R, Lacík I, Weir GC, Oberholzer J, Greiner DL, Langer R, Anderson DG. Size- and shape-dependent foreign body immune response to materials implanted in rodents and non-human primates. Nat Mater. 2015;14:643–51.

51. Boddupalli A, Zhu L, Bratlie KM. Methods for Implant Acceptance and Wound Healing: Material Selection and Implant Location Modulate Macrophage and Fibroblast Phenotypes. Adv Healthc Mater. 2016;

52. Anderson JM, McNally AK. Biocompatibility of implants: Lymphocyte/macrophage interactions. Semin Immunopathol. 2011;33:221–33.

53. Lago N, Yoshida K, Koch KP, Navarro X. Assessment of biocompatibility of chronically implanted polyimide and platinum intrafascicular electrodes. IEEE Trans Biomed Eng. 2007;54:281–90.

54. Damanik FFR, Rothuizen TC, van Blitterswijk C, Rotmans JI, Moroni L. Towards an in vitro model mimicking the foreign body response: tailoring the surface properties of biomaterials to modulate extracellular matrix. Sci Rep. 2014;4:6325.

55. Pacelli S, Manoharan V, Desalvo A, Lomis N, Jodha KS, Prakash S, Paul A. Tailoring biomaterial surface properties to modulate host-implant interactions: implication in cardiovascular and bone therapy. J Mater Chem B. Royal Society of Chemistry; 2015;4:1586–99.

**Figure captions**

**Figure 1. Surgical procedure**. (A) Photograph of the longitudinal device implanted (bottom) and the implantation needle used (above). (B) Needle used for the implantation piercing (arrowhead) the sciatic nerve (arrow) of a rat. (C) Device implanted (arrow points to the triangle base) in the sciatic nerve. Scale bar in (B-C) = 1mm.

**Figure 2. Histological evaluation of implanted nerves.** (A) Low and (B) high magnification images of semithin sections of sham (above) and implanted (below) nerves after 2 weeks. (C) Quantification of myelinated fibers in sham and implanted nerves. The dotted line indicates the mean number of intact tibial nerves. Scale bar in (A) = 200µm and (B) = 10µm.

**Figure 3. Histological progression of capsule tissue around the implants.** (A) Representative images of time progression of the capsule around polyimide implants. (B) No signs of tissue aggregation can be observed in sham nerves. (C) Measurements of capsule thickness along time. *$p<0.05$ vs 2weeks. Scale bar = 50µm.

**Figure 4. Tissue capsule development around the implant** (bottom). (A-F) Magnification of semithin sections showing changes in the capsule. At (A) day 1, erythrocytes (arrow) can be seen near the implant. After 4 days, 2 and 4 weeks (B-D) amoeboid cells (asterisks) are forming the capsule. After 8 and 16 weeks (E & F), the capsule is already compacted and spindle-shape cells (arrowheads) are seen within. (D-F) Representative transmission electron microscopy images taken at different time points with the amoeboid-shaped cells (asterisks) in the inner zone of the capsule at 2 weeks and the spindle-shaped cells (arrowheads) in the outer zone at 8 and 32 weeks. Insets of G-I show high-magnification view of changes in collagen matrix deposition at 2, 8 and 32 weeks. Scale bar = 10µm (A-F), 5µm (G-I), 2µm (insets).

# Figure 1

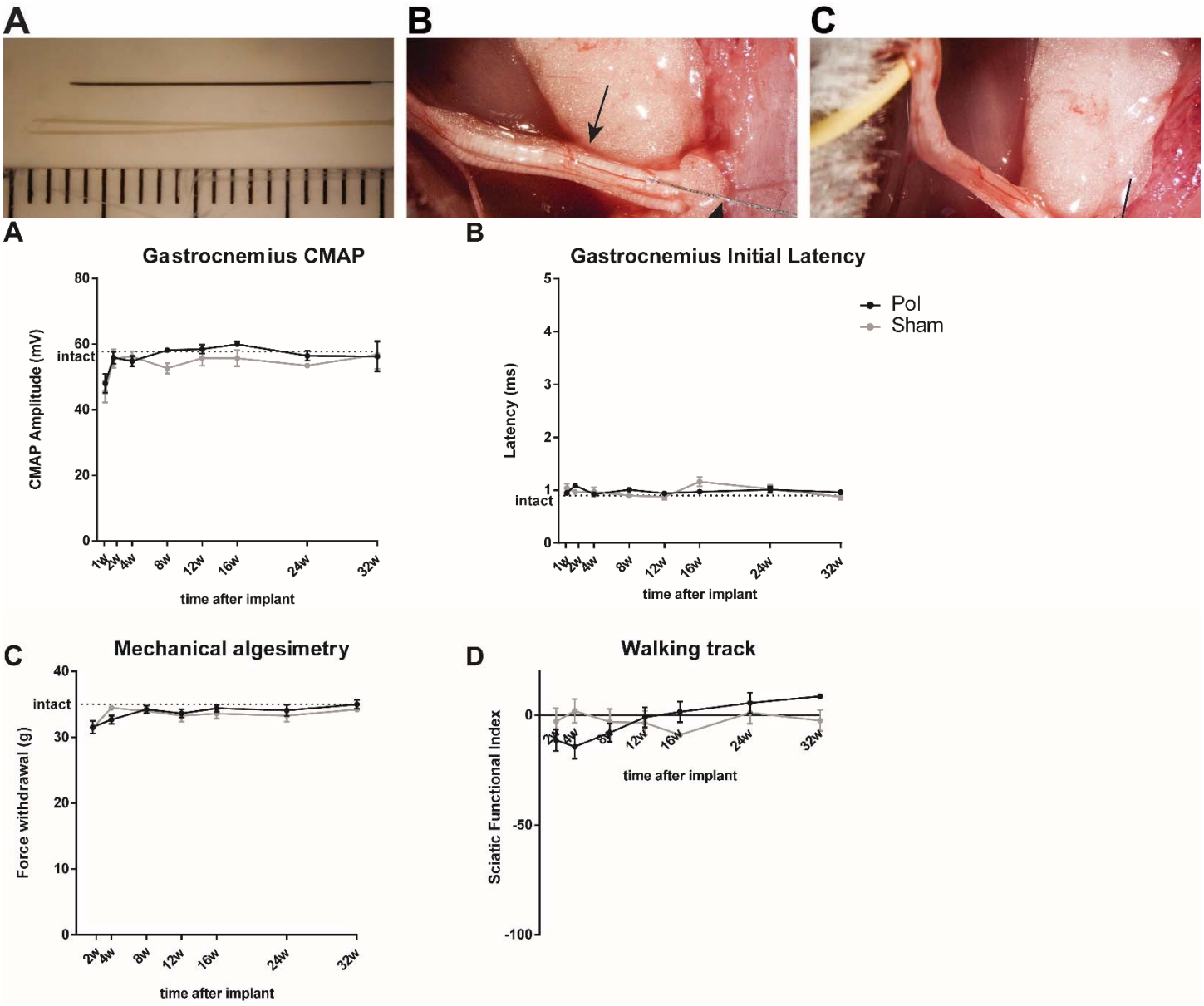
A
B
C
A
Gastrocnemius CMAP
CMAP Amplitude (mV)
intact
time after implant
B
Gastrocnemius Initial Latency
Pol
Sham
Latency (ms)
intact
time after implant
C
Mechanical algesimetry
Force withdrawal (g)
intact
time after implant
D
Walking track
Sciatic Functional Index
time after implant

# Figure 2

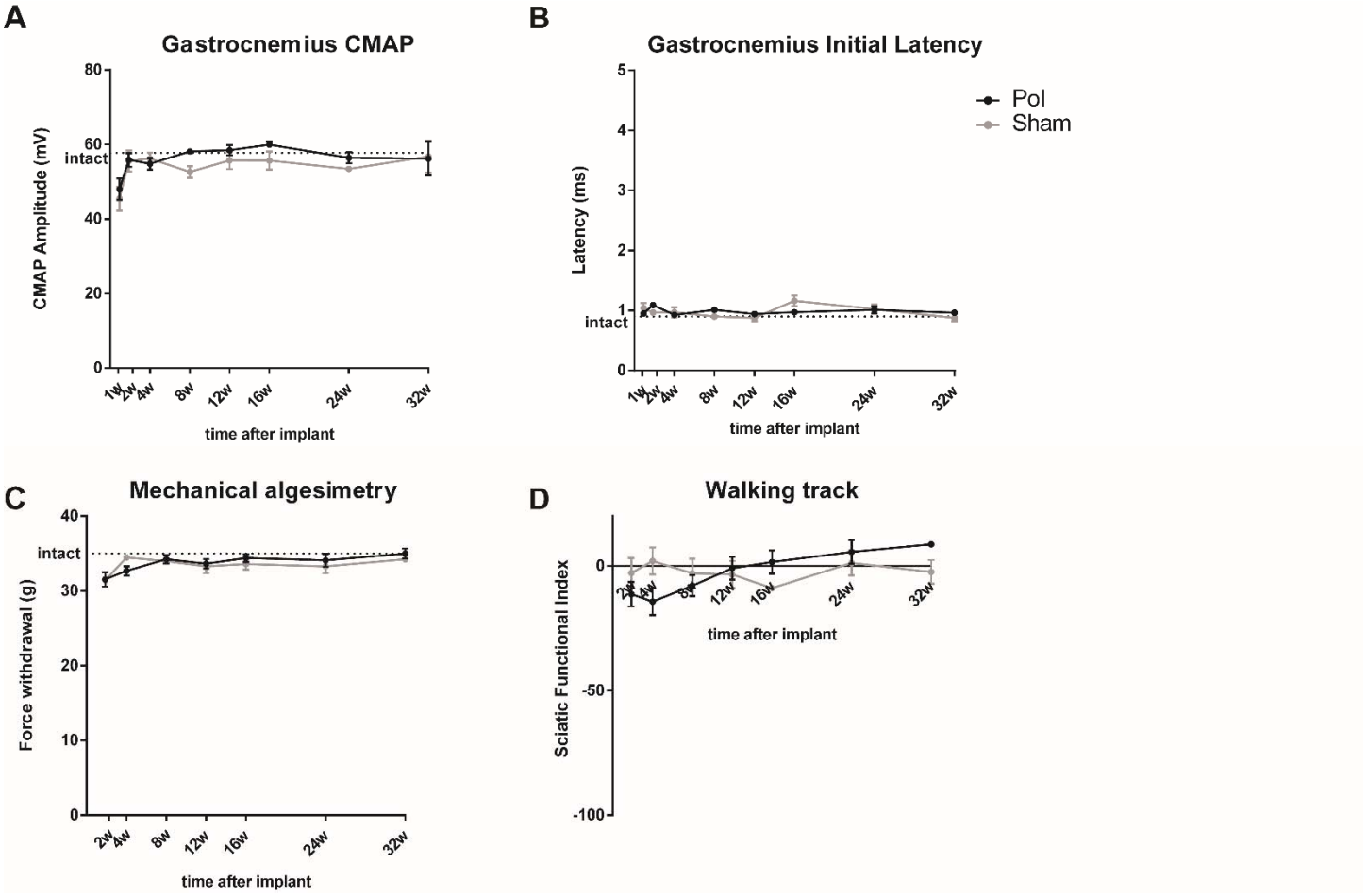
A
Gastrocnemius CMAP
CMAP Amplitude (mV)
intact
time after implant
B
Gastrocnemius Initial Latency
Latency (ms)
intact
Pol
Sham
time after implant
C
Mechanical algesimetry
Force withdrawal (g)
intact
time after implant
D
Walking track
Sciatic Functional Index
time after implant

# Figure 3

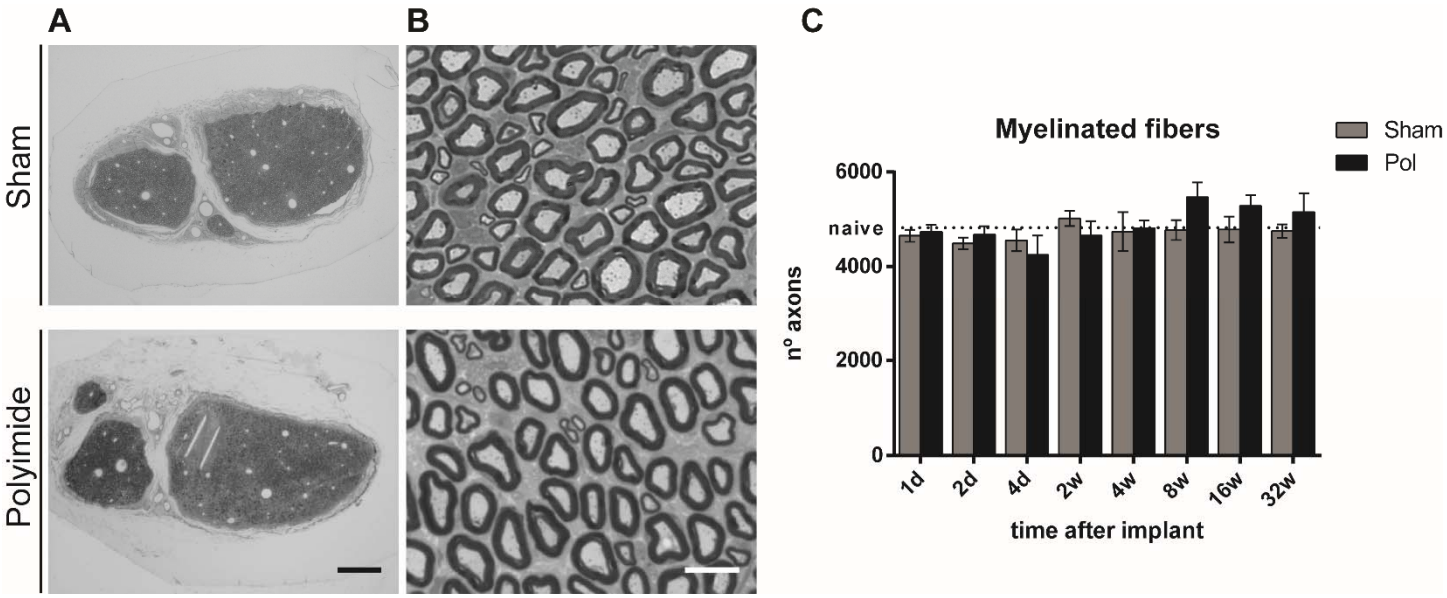
A
B
C
Sham
Polyimide
Myelinated fibers
Sham
Pol
6000
naive
4000
2000
0
n° axons
1d
2d
4d
2w
4w
8w
16w
32w
time after implant

**Figure 4**

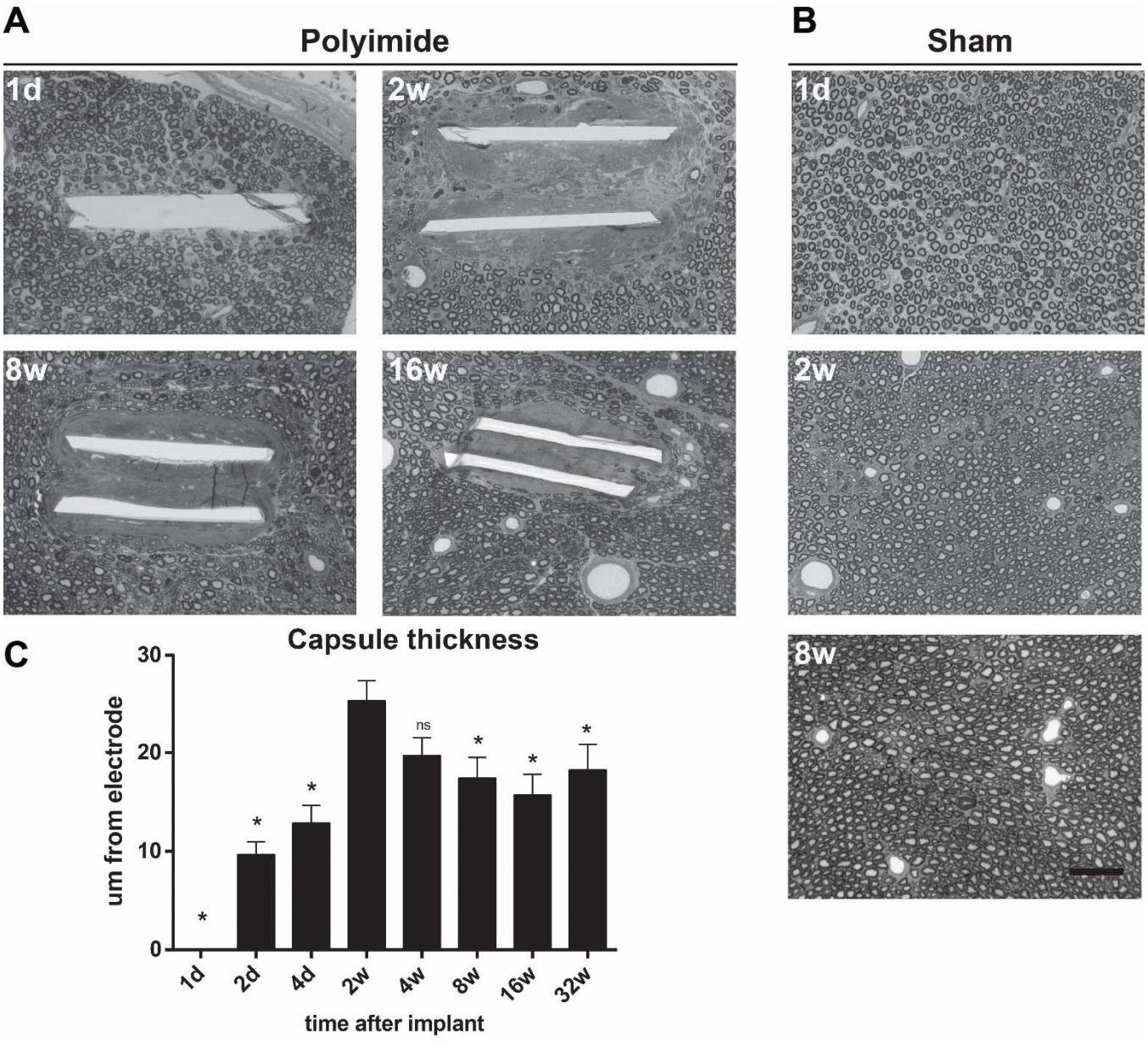
A
Polyimide
1d
2w
8w
16w
B
Sham
1d
2w
8w
C
Capsule thickness
um from electrode
30
20
10
0
ns
*
1d
2d
4d
2w
4w
8w
16w
32w
time after implant

**Figure 5**

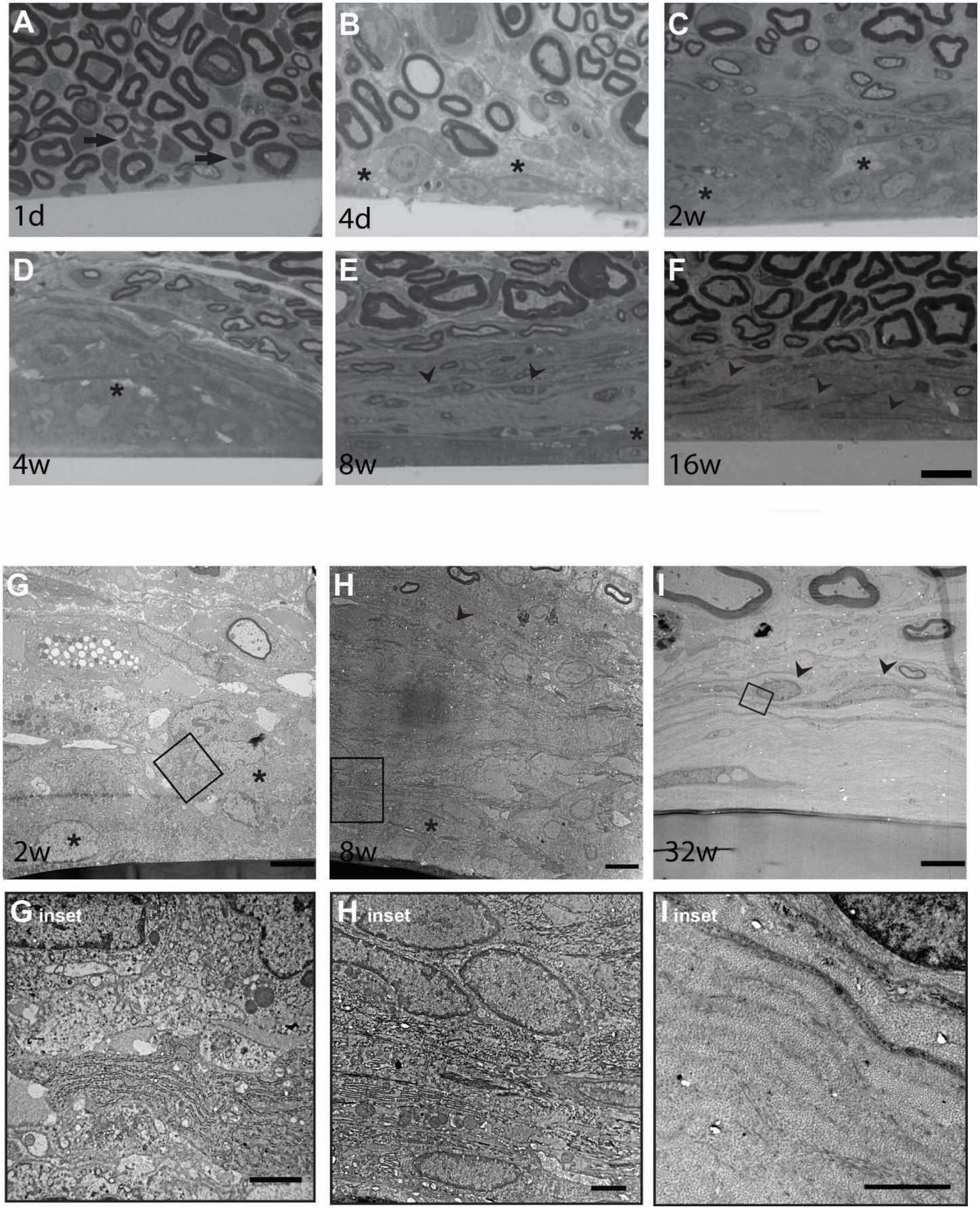

# Figure 6

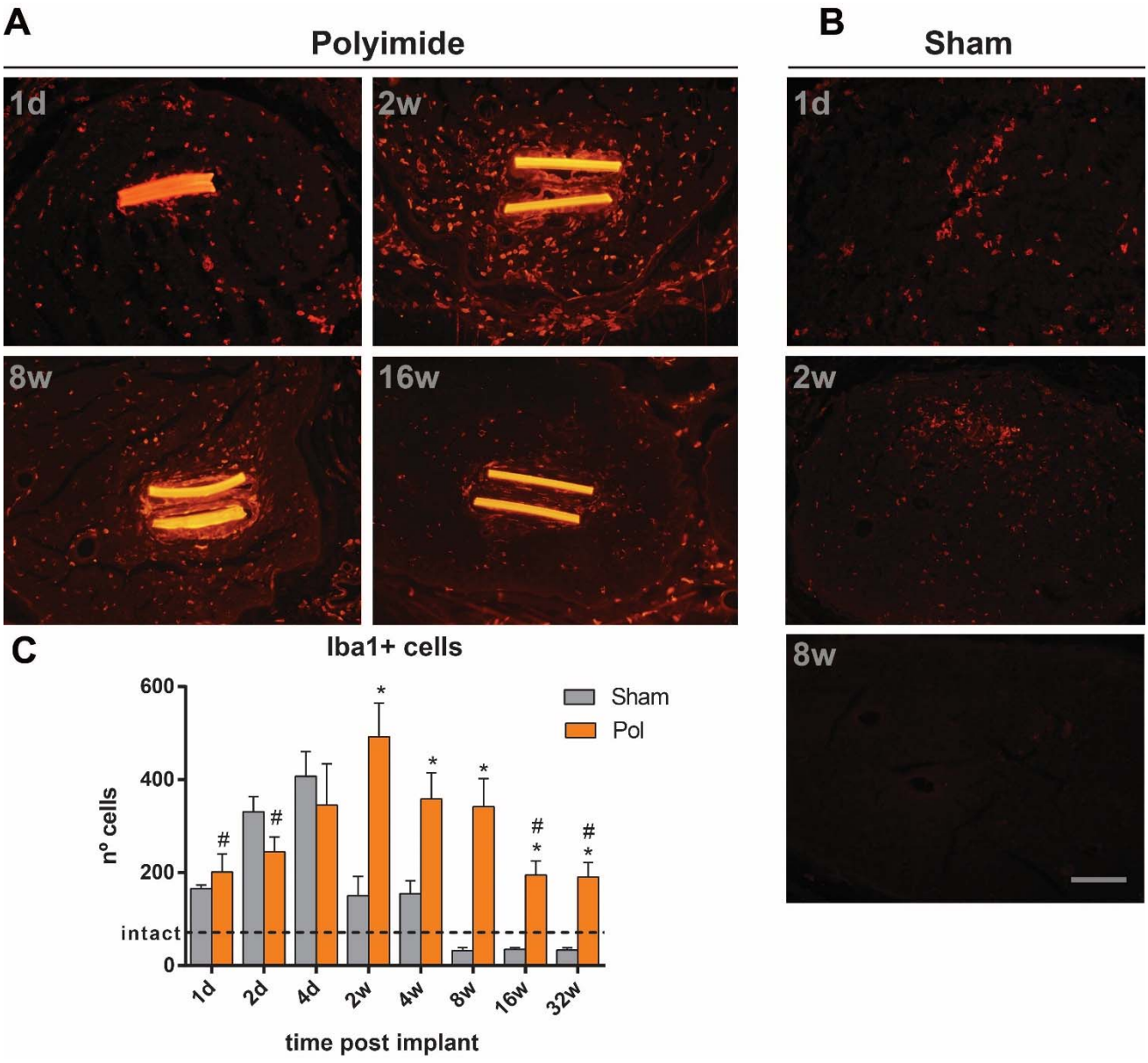
A
Polyimide
1d
2w
8w
16w
B
Sham
1d
2w
8w
C
Iba1+ cells
Sham
Pol
n° cells
600
400
200
intact
0
1d
2d
4d
2w
4w
8w
16w
32w
time post implant

**Figure 7**

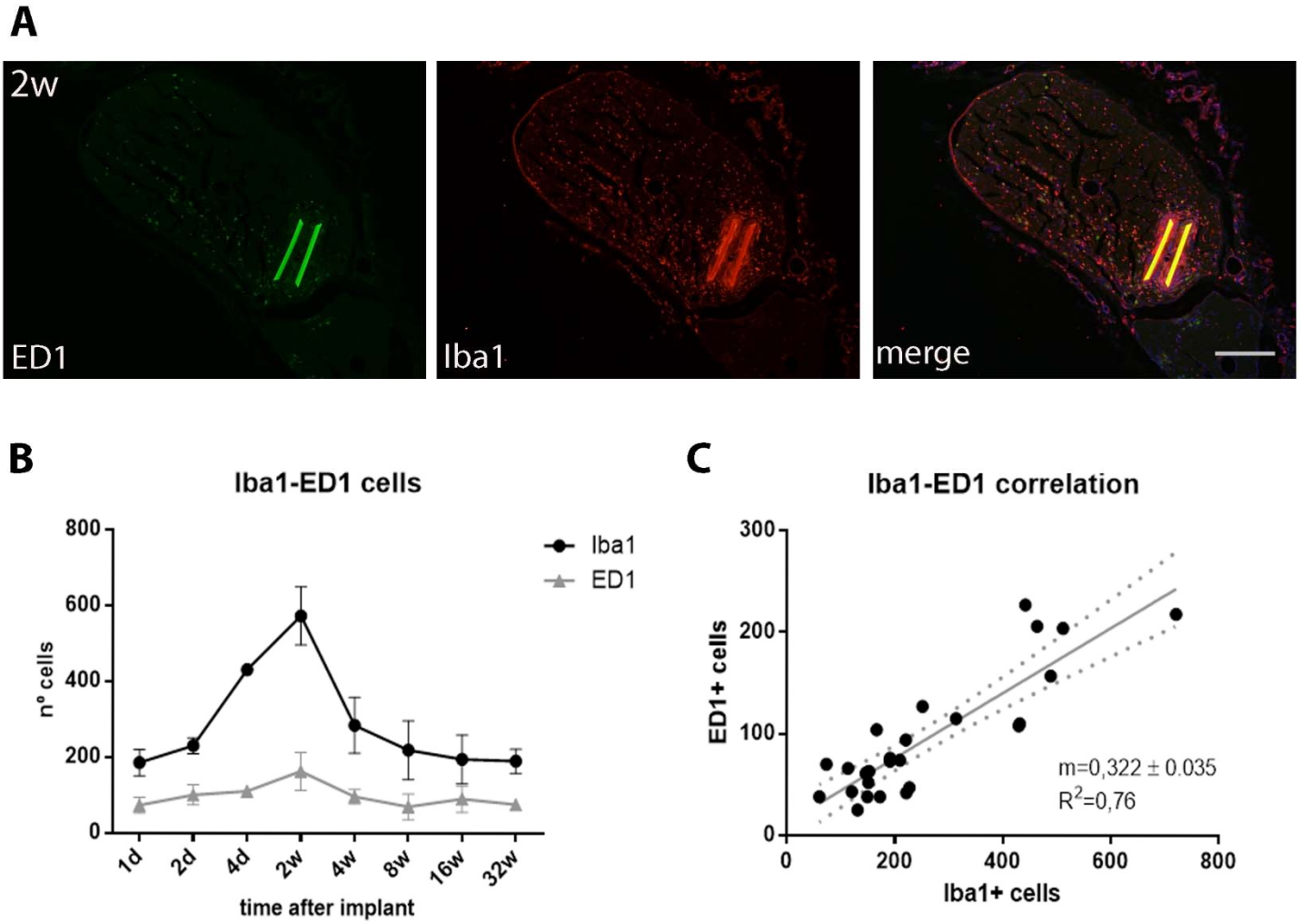
A
2w
ED1
Iba1
merge
B
Iba1-ED1 cells
nº cells
800
600
400
200
0
Iba1
ED1
1d
2d
4d
2w
4w
8w
16w
32w
time after implant
C
Iba1-ED1 correlation
ED1+ cells
300
200
100
0
0
200
400
600
800
Iba1+ cells
m=0,322 ± 0.035
R2=0,76

**Figure 8**

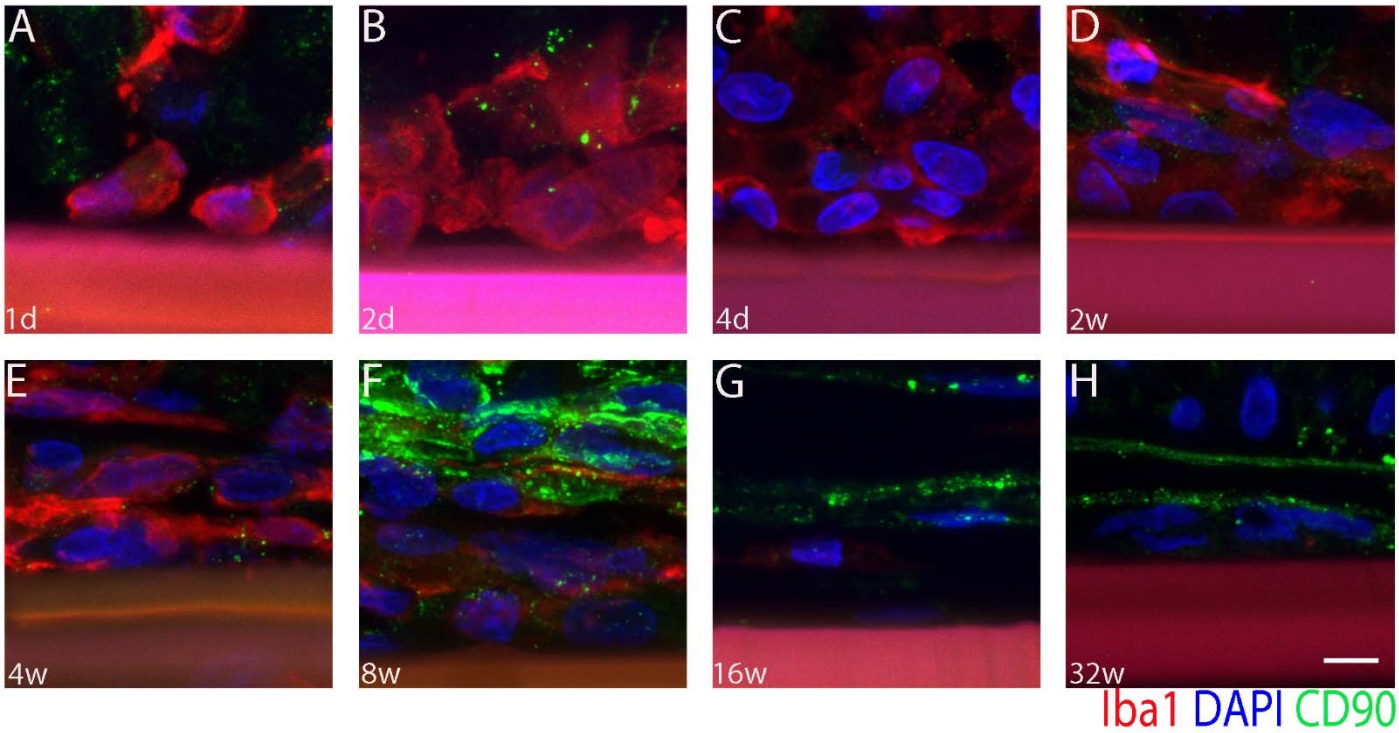

# Figure 9

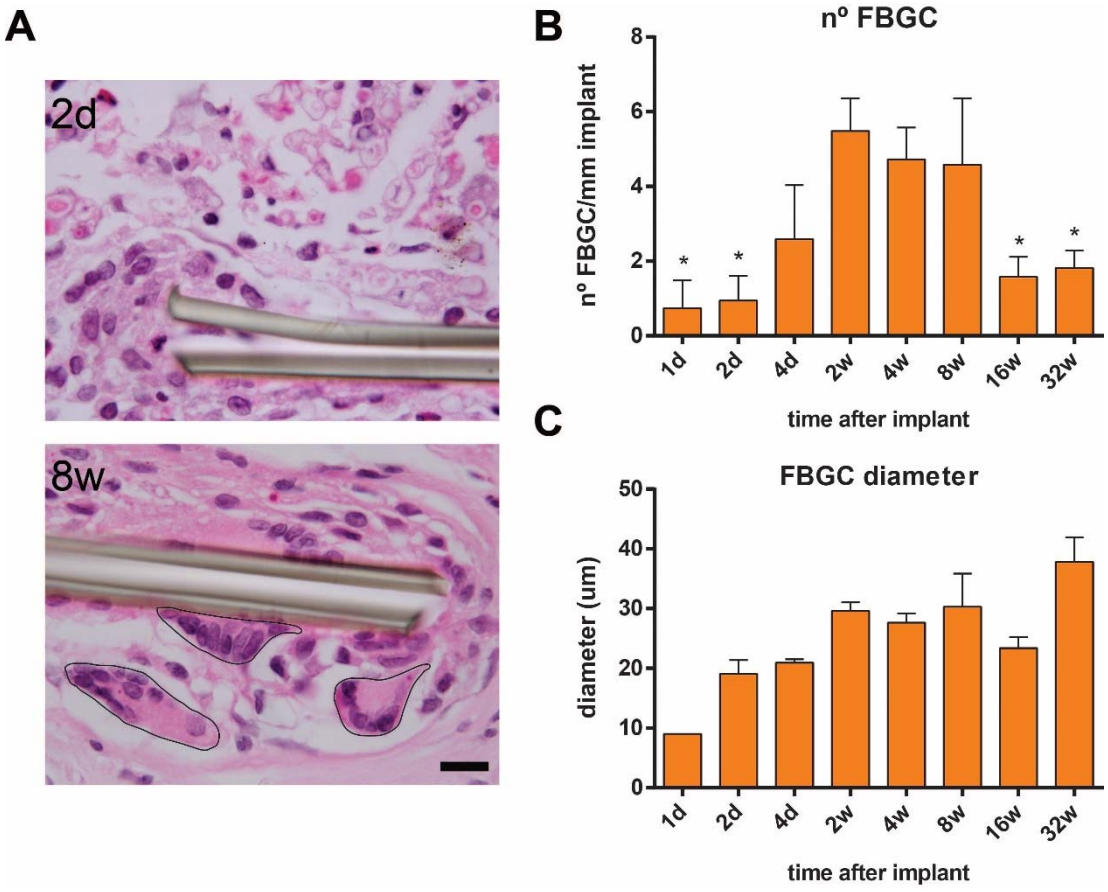
A
2d
8w
B
nº FBGC
nº FBGC/mm implant
0
2
4
6
8
*
*
*
*
1d
2d
4d
2w
4w
8w
16w
32w
time after implant
C
FBGC diameter
diameter (um)
0
10
20
30
40
50
1d
2d
4d
2w
4w
8w
16w
32w
time after implant

**Figure 5. Inflammatory cells in the implanted nerves.** Representative images of macrophages labelled with Iba1 at different times points in (A) implanted and (B) sham nerves. (C) Quantification of the number of Iba1 positive cells along time in implanted and sham animals. Dotted line indicates the mean of intact nerves.*p<0.05 vs sham. #p<0.05 vs 2weeks. Scale bar = 100 μm.

**Figure. 6. Cellular events in the tissue capsule around the device**. Representative confocal images of cells in the capsule from 1 day to 32 weeks. Macrophages (red) are in contact with the device until 16 weeks. Fibroblasts (green) appear at 4-8 weeks and are located in the periphery of the capsule, in contact with nerve fibres. Scale bar = 15 μm.

**Figure. 7. Foreign body giants cells** as a hallmark of the FBR. (A) Presence of FBGC in the surface of the device observed with Hematoxilin-Eosin at different time points. (B) Number and (C) diameter of FBGC on the device along time. *p<0.05 vs 2weeks. Scale bar = 15 μm.

**Supplementary figure 1. Functional evaluation of implanted nerves.** No alterations were found in the (A) amplitude or (B) initial latency of the gastrocnemius compound muscle action potential (CAMP) of implanted and sham animals. (C) Pain threshold assess by Von Frey mechanical algesimetry in the central area of the paw. (D) SFI of sham and implanted animals. Dotted lines indicate values from intact animals.

**Supplementary figure 2. ED1-Iba1 macrophage staining over time.** (A) Representative images of ED1 (green) and Iba1 (red) labeling after 2 weeks of implant, cell nuclei can be seen in blue after DAPI staining. (B) Quantification of the number of ED1 positive cells and Iba1 positive cells over time. (C) Correlation between ED1 and Iba1 positive cells. The solid

grey line represents the linear regression (slope significantly different from zero, $p<0,001$), while the dotted line represents the 95% confidence interval. Scale bar = 200 μm.